The EMBO Journal Vol. 22 No. 3 pp. 676–688, 2003

ATP binding by glutamyl-tRNA synthetase is switched to the productive mode by tRNA binding

Shun-ichi Sekine[1], Osamu Nureki[1,2], Daniel Y.Dubois[3], Stéphane Bernier[4], Robert Chênevert[4], Jacques Lapointe[3], Dmitry G.Vassylyev[1,5] and Shigeyuki Yokoyama[1,2,5,6]

[1]Cellular Signaling Laboratory and Structurome Group, RIKEN Harima Institute at SPring-8, 1-1-1 Kouto, Mikazuki-cho, Sayo, Hyogo 679-5148, [2]Department of Biophysics and Biochemistry, Graduate School of Science, University of Tokyo, 7-3-1 Hongo, Bunkyo-ku, Tokyo 113-0033, [6]Genomic Sciences Center, RIKEN Yokohama Institute, 1-7-22 Suehiro-cho, Tsurumi, Yokohama 230-0045, Japan and [3]Départements de Biochimie et Microbiologie and [4]Chimie, Faculté des Sciences et de Génie, CREFSIP, Université Laval, Québec, Canada G1K 7P4

[5]Corresponding authors
e-mail: dmitry@yumiyoshi.harima.riken.go.jp or yokoyama@biochem.s.u-tokyo.ac.jp

Aminoacyl-tRNA synthetases catalyze the formation of an aminoacyl-AMP from an amino acid and ATP, prior to the aminoacyl transfer to tRNA. A subset of aminoacyl-tRNA synthetases, including glutamyl-tRNA synthetase (GluRS), have a regulation mechanism to avoid aminoacyl-AMP formation in the absence of tRNA. In this study, we determined the crystal structure of the 'non-productive' complex of *Thermus thermophilus* GluRS, ATP and L-glutamate, together with those of the GluRS·ATP, GluRS·tRNA·ATP and GluRS·tRNA·GoA (a glutamyl-AMP analog) complexes. In the absence of $tRNA^{Glu}$, ATP is accommodated in a 'non-productive' subsite within the ATP-binding site, so that the ATP α-phosphate and the glutamate α-carboxyl groups in GluRS·ATP·Glu are too far from each other (6.2 Å) to react. In contrast, the ATP-binding mode in GluRS·tRNA·ATP is dramatically different from those in GluRS·ATP·Glu and GluRS·ATP, but corresponds to the AMP moiety binding mode in GluRS·tRNA·GoA (the 'productive' subsite). There-fore, tRNA binding to GluRS switches the ATP-binding mode. The interactions of the three $tRNA^{Glu}$ regions with GluRS cause conformational changes around the ATP-binding site, and allow ATP to bind to the 'productive' subsite.

Keywords: aminoacylation/aminoacyl-tRNA synthetase/ribonucleoprotein/tRNA/X-ray crystallography

Introduction

The fidelity of genetic code translation is ensured by a set of aminoacyl-tRNA synthetases (aaRSs), each of which catalyzes the coupling of its specific tRNA(s) and amino acid with a high degree of accuracy. In general, aminoacylation is a two-step event. In the first step, an aaRS 'activates' the amino acid using ATP and Mg^{2+}, yielding an enzyme-bound high energy intermediate, the aminoacyl-adenylate (aa-AMP). In the second step, the aminoacyl moiety is transferred from the aa-AMP to the 3′-terminal adenosine of tRNA. The aaRSs are divided into two classes, each consisting of 10 enzymes, on the basis of the two distinct ATP-binding cores (Eriani *et al*., 1990; Cusack, 1995). The class I ATP-binding site is formed with the conserved HIGH (His-Ile-Gly-His) and KMSKS (Lys-Met-Ser-Lys-Ser) sequence motifs, while the class II ATP-binding site is formed with three conserved motifs.

Three of the class I aaRSs, the glutamyl-, glutaminyl- and arginyl-tRNA synthetases (GluRS, GlnRS and ArgRS, respectively), are known to share a special property: they catalyze the first step, amino acid activation, only in the presence of their cognate tRNA(s) (Ravel *et al*., 1965; Mitra and Mehler, 1966, 1967; Deutscher, 1967; Lee *et al*., 1967; Mehler and Mitra, 1967; Lapointe and Söll, 1972). As exceptions, several bacteria and archaea have the class I-type lysyl-tRNA synthetase (LysRS-I) instead of the class II-type LysRS (LysRS-II) (Ibba *et al*., 1997a,b). LysRS-I is structurally related to GluRS (Terada *et al*., 2002), and does not catalyze Lys-AMP formation in the absence of tRNA (Ibba *et al*., 1999). For these synthetases, the tRNA serves as the activator in the first step, and as the substrate in the second step of aminoacylation (Ravel *et al*., 1965; Mitra and Mehler, 1966, 1967; Lee *et al*., 1967; Mehler and Mitra, 1967; Kern and Lapointe, 1980). The activator function requires the integrity of the 3′ terminus of the tRNA, and chemical modification of this terminus abolishes the activity (Ravel *et al*., 1965; Mitra and Mehler, 1966; Lee *et al*., 1967; Kern and Lapointe, 1979). Glutamyl-AMP (Glu-AMP) is chemically unstable, and therefore it has been proposed that the tRNA-dependent glutamic acid activation is required to minimize ATP consumption, which would otherwise result from the spontaneous breakdown of the activated amino acid (Deutscher, 1967).

On the basis of the crystal structure of the ternary complex of the *Escherichia coli* GlnRS, $tRNA^{Gln}$ and ATP, it has been proposed that a characteristic structural element of GlnRS transfers the signal from the anticodon to the catalytic site (Rould *et al*., 1989, 1991). It was also reported that the 2′-hydroxyl group of the tRNA terminal adenosine is close to the bound ATP molecule (Perona *et al*., 1993). In the structure of another complex of GlnRS and $tRNA^{Gln}$ with QSI (an analog of Gln-AMP), the 2′- and 3′-hydroxyl groups of the terminal adenosine form hydrogen bonds with the NH of the sulfamoyl group and the α-ammonium group, respectively, of QSI, indicating that the tRNA itself is involved in the Gln-AMP-binding site (Rath *et al*., 1998). In addition, the structures of the *Thermus thermophilus* GluRS (Nureki *et al*., 1995) and the GluRS·$tRNA^{Glu}$ complex (Sekine *et al*., 2001), the

Table I. Crystallographic data and refinement statistics

Complex	1	2	3	4
Code	ERS/ATP/Glu	ERS/ATP	ERS/tRNA/ATP	ERS/tRNA/GoA
Macromolecules	GluRS	GluRS	GluRS and $tRNA^{Glu}$	GluRS and $tRNA^{Glu}$
Ligands	ATP and L-Glu	ATP	ATP	Glutamol-AMP
Data set				
SPring-8 BL station	BL41XU	BL45PX	BL41XU	BL41XU
Space group	$P2_12_12_1$	$P2_12_12_1$	$C222_1$	$C222_1$
Unit cell dimensions	a = 81.92	a = 82.72	a = 110.69	a = 110.49
	b = 82.62	b = 84.06	b = 219.12	b = 219.87
	c = 83.11 Å	c = 83.45 Å	c = 135.22 Å	c = 135.12 Å
Resolution (Å)	40–1.8	50–1.9	50–2.4	50–2.1
Total reflections	208 385	175 753	247 929	426 837
Unique reflections	49026	46014	59840	92817
Completeness (%)	91.7 (92.8)[a]	98.3 (96.9)	91.2 (80.8)	96.4 (88.5)
R_{merge}[b] (%)	6.3 (44.4)[c]	5.9 (36.7)	7.2 (35.7)	7.4 (34.2)
Refinement statistics				
Resolution (Å)	40–1.8	50–1.9	50–2.4	50–2.1
Reflections	48 560	45 764	58 889	90 631
R_{cryst}[d] (%)	19.9	20.9	21.3	21.9
R_{free}[d] (%)	22.7	23.6	25.7	25.9
No. of protein atoms	3813	3813	7626	7626
No. of tRNA atoms	–	–	3194	3194
No. of water atoms	352	344	505	739
No. of ligand atoms	45	35	64	76
R.m.s.d. bonds (Å)	0.005	0.005	0.006	0.006
R.m.s.d. angles (°)	1.2	1.2	1.3	1.2
R.m.s.d. improper angles (°)	0.85	0.84	1.5	1.4
Ramachandran plot (most favorable region) (%)	94.8	95.5	93.7	93.7

[a]The completeness in the highest resolution shell is given in parentheses.
[b]$R_{merge} = \Sigma|I - <I>|/\Sigma I$, where I is the observed intensity of reflections.
[c]R_{merge} in the highest resolution shell is given in parentheses.
[d]$R_{cryst,\ free} = \Sigma|F_{obs} - F_{calc}|/\Sigma F_{obs}$, where the crystallographic R-factor is calculated including and excluding refinement reflections. In each refinement, free reflections consist of 5% of the total number of reflections.

Saccharomyces cerevisiae ArgRS·L-arginine, ArgRS·$tRNA^{Arg}$ and ArgRS·$tRNA^{Arg}$·L-arginine complexes (Cavarelli *et al*., 1998; Delagoutte *et al*., 2000), the *T.thermophilus* ArgRS (Shimada *et al*., 2001) and the *Pyrococcus horikoshii* LysRS-I and its complex with L-lysine (Terada *et al*., 2002) have been determined so far, but the mechanisms that prevent these four synthetases from catalyzing the amino acid activation in the absence of tRNA are not understood.

In the present study, we determined four crystal structures of GluRS from *T.thermophilus* in the following complexes: GluRS·ATP·L-glutamate, GluRS·ATP, GluRS·$tRNA^{Glu}$·ATP and GluRS·$tRNA^{Glu}$·glutamol-AMP (GoA, a stable analog of Glu-AMP) (ERS/ATP/Glu, ERS/ATP, ERS/tRNA/ATP and ERS/tRNA/GoA, respectively; Table I). The high resolution structures of these *T.thermophilus* GluRS complexes showed that the ATP-binding site of GluRS has two distinct 'subsites'. In particular, the structure of the ternary GluRS·ATP·L-glutamate complex clearly shows that this complex is really 'non-productive': the ATP bound in this mode (the 'non-productive' subsite) in the absence of $tRNA^{Glu}$ is too far from the glutamate to react with it. In the presence of $tRNA^{Glu}$, ATP binds to the 'productive' subsite, which is also used for binding the AMP moiety of the Glu-AMP analog. Interactions with the three regions of $tRNA^{Glu}$ cause conformational changes around the ATP-binding site of GluRS, thus switching the binding mode.

Results and discussion

Structure determination

The crystal structure of ERS/ATP/Glu (complex 1, Table I) was solved by molecular replacement using the free GluRS structure (Nureki *et al*., 1995) as the search model, and was refined against data to 1.8 Å resolution (Figure 1A). The crystallographic asymmetric unit contains one ERS/ATP/Glu. Under nearly the same conditions, the ERS/ATP crystals (complex 2, Table I) were obtained in the absence of glutamate. The structure was determined by molecular replacement, and refined to 1.9 Å resolution (Table I). The overall enzyme structures in ERS/ATP/Glu and ERS/ATP are almost the same; the root mean square deviation (r.m.s.d.) is 0.54 Å over all of the protein atoms.

The ERS/tRNA/ATP (Figure 1B) and ERS/tRNA/GoA structures (complexes 3 and 4) were determined and refined to 2.4 and 2.1 Å resolution, respectively (Table I). Each structure contains two nearly identical complexes (a and b) in the crystallographic asymmetric unit. Herein, the discussion is based on the complex a structures, unless otherwise specified. The overall enzyme and tRNA structures in ERS/tRNA/ATP and ERS/tRNA/GoA are practically the same (r.m.s.d. = 0.41 Å over all of the protein and RNA atoms). Both of the complexes are superposable on the previous GluRS·$tRNA^{Glu}$ binary complex (ERS/tRNA) (Sekine *et al*., 2001) (r.m.s.d.

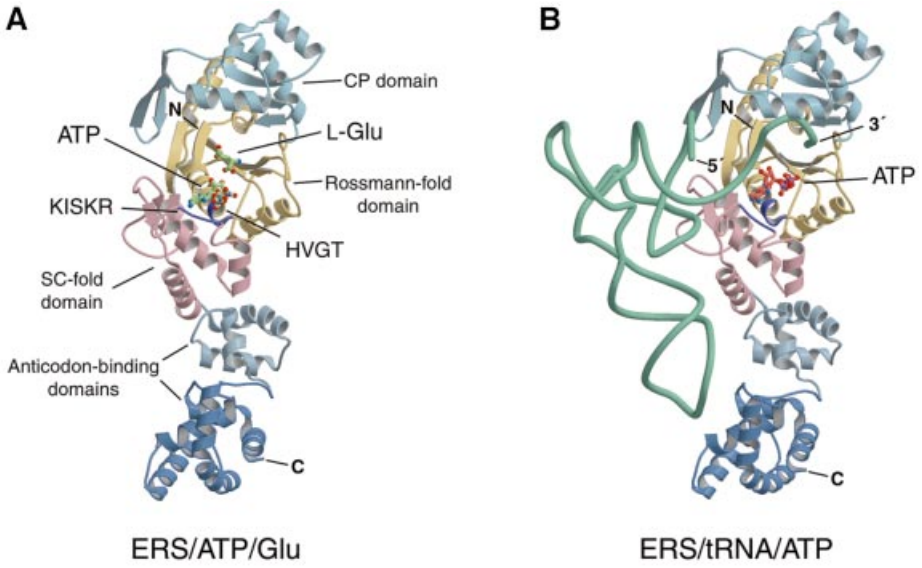

Fig. 1. *Thermus thermophilus* GluRS crystal structures. (**A**) Ribbon representation of the ERS/ATP/Glu structure. Five domains, the Rossmann fold (1), connective peptide (or acceptor-binding) (2), stem-contact fold (3) and two anticodon-binding (4 and 5) domains, are colored khaki, light blue, pink, steel blue and deep blue, respectively. The HVGT and KISKR motifs of GluRS are highlighted in purple. The ATP and glutamate molecules in the GluRS catalytic pocket are shown in green. (**B**) Overall structure of ERS/tRNA/ATP. The ATP and $tRNA^{Glu}$ molecules in the complex are shown in orange and turquoise, respectively. These figures were produced using the MOLSCRIPT (Kraulis, 1991) and RASTER3D (Merritt and Murphy, 1994) programs.

~0.71 Å over all of the protein and RNA atoms for both comparisons).

Herein, these GluRS structures are compared by superposition of the enzyme catalytic cores (domains 1 and 3). The catalytic domain structures in the ERS/ATP/Glu, ERS/ATP and ERS/tRNA/ATP structures (complexes 1–3) were fitted to those in the ERS/tRNA/GoA (complex 4) as a reference, by using the LSQKAB program (CCP4, 1994) (r.m.s.d. values are 0.49, 0.50 and 0.22 Å, respectively, for 156 Cα atoms). Flexible regions were excluded from the calculations. The differences thus found are described in the following sections.

Conformational changes of GluRS upon $tRNA^{Glu}$ binding

A comparison of the tRNA-free and tRNA-bound GluRS structures reveals the tRNA-dependent conformational changes within the domain linkers and loops (Figure 2A). For the specific interaction of the two anticodon-binding domains (4 and 5) with the tRNA anticodon loop (Sekine *et al.*, 2001), these domains are reoriented, without changing their folds, by an ~6° rotation of domain 4 relative to domain 3 (the SC fold domain), and by an ~8° rotation of domain 5 relative to domain 4 (Figure 2A). In the present crystal protein structures, we could not see any direct structural linkage that may transmit the anticodon-binding signal to the catalytic site, in contrast to the structure of the *E.coli* GlnRS·tRNA·ATP complex (QRS/tRNA/ATP) (Rould *et al.*, 1989, 1991).

The CP domain (domain 2) also changes its orientation upon $tRNA^{Glu}$ binding (Figure 2A). It rotates by ~7° relative to domain 1, and thus binds the 3′ acceptor end of the tRNA molecule. The $tRNA^{Glu}$ C74 is trapped by a pocket formed on the CP domain, without stacking on the other bases in the 3′-terminal region (Figure 2B). The C74 base is recognized specifically by interactions mainly with the main chains of Glu107 and Ser181, while the C74 phosphate interacts with Arg147. Here, the 3′ end is bent back toward the enzyme active site, resulting in a hairpin conformation. In the GluRS-bound $tRNA^{Glu}$, the G1·C72 base pair of the acceptor stem is intact (Figure 2B), in contrast to the disrupted U1·A72 base pair in the *E.coli* GlnRS-bound $tRNA^{Gln}$ (Rould *et al.*, 1989). Correspondingly, GlnRS possesses a unique insertion structure that interacts with A72, whereas GluRS does not (Nureki *et al.*, 1995).

The A73 base does not interact with any protein residues, but is involved in a stacking array formed by the A73, C75 and A76 bases and the Trp209 and Tyr187 rings (Figure 2B). The 2′-hydroxyl group of C75 interacts with the conserved Asp44 and Arg47 side chains on the Rossmann fold (domain 1). The phosphate group of the terminal adenosine (A76) interacts with Lys180 and Tyr187. The 5′-hydroxyl group of A76 interacts with the Thr43 side chain. In the previous structure of ERS/tRNA (Sekine *et al.*, 2001), the electron density corresponding to C75 and A76 of the tRNA molecule was poor. Finally, tRNA-induced conformational changes are observed in the loop of residues 206–209 in the Rossmann fold domain and in the 'KMSKS' region in the SC fold domain (Figure 2A), which are described below.

ATP and Glu binding in the absence of tRNA

The 1.8 Å resolution structure of ERS/ATP/Glu (Table I; Figure 1A) was the first to reveal both the enzyme-bound ATP and amino acid substrates without a reaction (Figure 3A). This is in good agreement with the observations that the *E.coli* and *T.thermophilus* GluRSs are

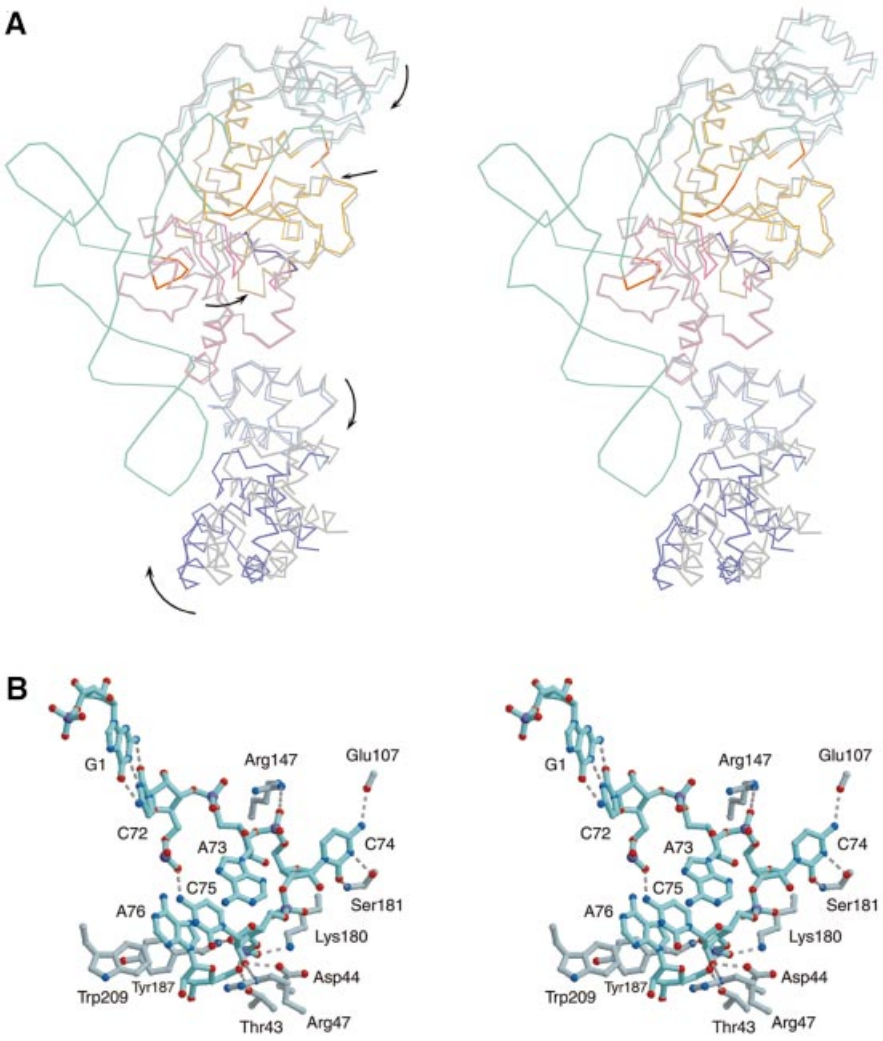

Fig. 2. Conformational changes within GluRS upon $tRNA^{Glu}$ binding. (**A**) The ERS/tRNA/GoA backbone structure was superposed on that of ERS/ATP/Glu by the enzyme catalytic core (domains 1 and 3) (stereo view). The entire ERS/ATP/Glu structure is colored gray, while the ERS/tRNA/GoA structure is colored as in Figure 1B. The arrows indicate the tRNA-induced conformational changes within GluRS. Three tRNA regions involved in the enzyme active site rearrangement are highlighted in orange. (**B**) A stereo view showing the 3′-terminal region of the $tRNA^{Glu}$ in ERS/tRNA/GoA, and its interactions with GluRS. These interactions are the same as those observed in ERS/tRNA/ATP.

absolutely inactive in the absence of their cognate $tRNA^{Glu}$ (Lapointe and Söll, 1972; S.Sekine and S.Yokoyama, unpublished). The ATP-Mg^{2+} substrate interacts intensively with the region including the ^{243}KISKR^{247} motif (the 'KMSKS' motif of the *T.thermophilus* GluRS) (Figure 3B). The KISKR loop has a different conformation from that within the substrate-free GluRS (Nureki *et al*., 1995) (not shown), which suggests an induced fit upon ATP binding. The adenine base is accommodated in a hydrophobic pocket formed by His15, Tyr20, Leu235, Leu236 and Ile244 (Figure 3B; Supplementary figure 1, available at *The EMBO Journal* Online). The N1 and N6 of the adenine make hydrogen bonds with the main chains of Leu236 and Ile244. The ATP phosphate groups hydrogen-bond extensively with Lys243, Ser245, Lys246 and Arg247. The Mg^{2+} ion has a unique octahedral coordination by the ATP α-, β- and γ-phosphate oxygen atoms and the three water molecules, which fix the ATP phosphate conformations (Figure 3A and B). The Glu208 and Lys243 side chains interact with the Mg^{2+} ion through water molecules. The 2′-hydroxyl group of the ATP ribose in the C2′-*endo* conformation interacts with the Glu208 and Trp209 side chains, while the back of the ATP interacts with the ^{15}HVGT^{18} motif (the 'HIGH' motif of the *T.thermophilus* GluRS).

On the other hand, the glutamate molecule lies along a β-strand, and its α-ammonium group hydrogen-bonds with the main chain of Ala7 and the side chains of Ser9 and Glu41 (Figures 3C and 4A). Four residues, Arg5, Tyr187, Asn191 and Arg205, constitute a pocket complementary to the γ-carboxyl group of glutamate, which determines the amino acid specificity. Remarkably, the α-carboxyl group of glutamate and the α-phosphate group of ATP are 6.2 Å apart (Figure 4A), and therefore are too far from each other to react. The glutamate α-carboxyl group instead interacts with the 3′-hydroxyl group of the ATP ribose. It should be noted that the position and the conformation of the ATP molecule in ERS/ATP/Glu are identical to those in ERS/

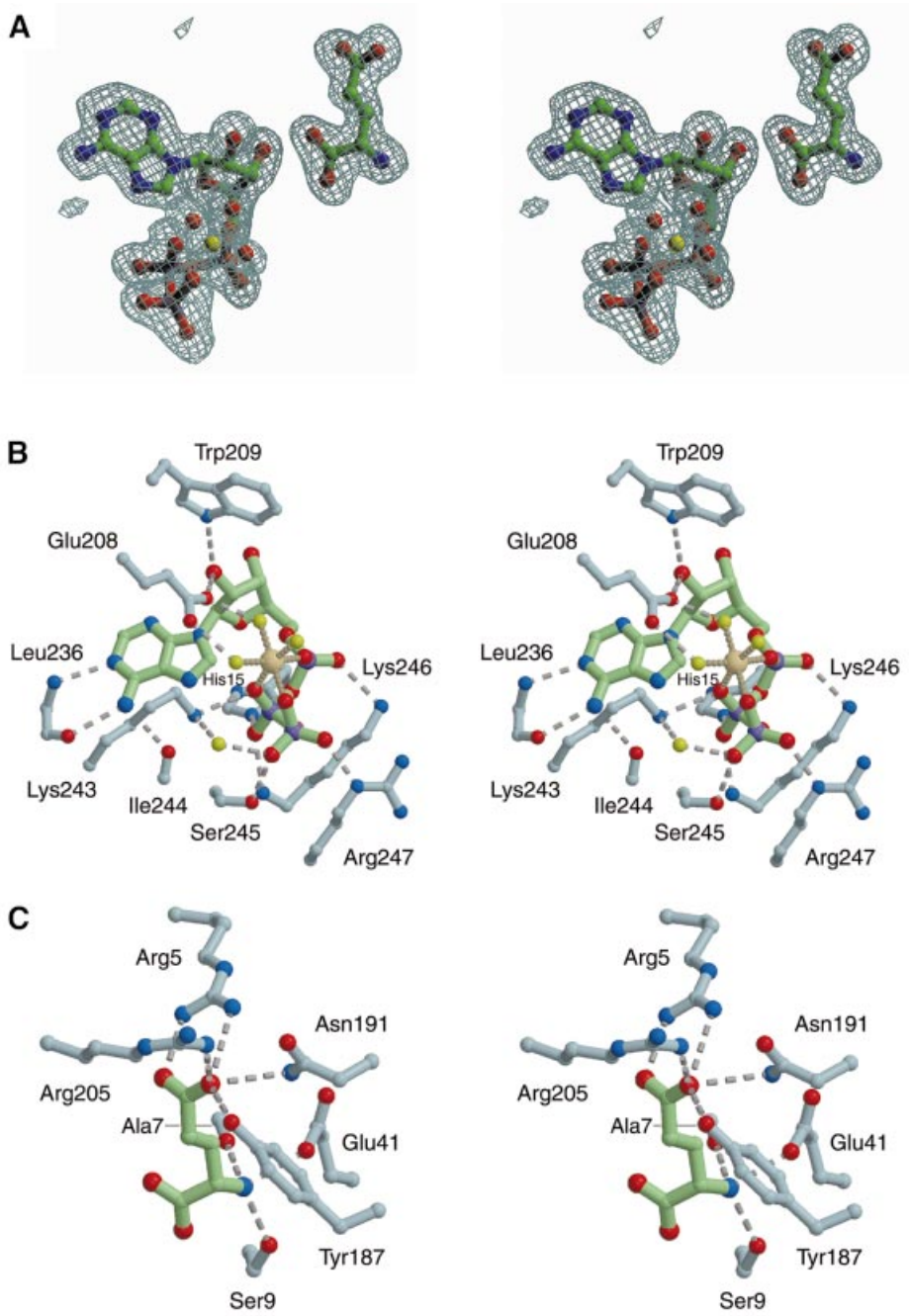

Fig. 3. The ATP and glutamate molecules in ERS/ATP/Glu. (**A**) A stereo view of the electron density, showing the ATP-Mg^{2+} and glutamate molecules in ERS/ATP/Glu. An annealed $|F_o - F_c|$ omit electron density map was calculated using all of the data from 40 to 1.8 Å resolution and the complex model without the ATP-Mg^{2+} and glutamate. The refined models of the ATP-Mg^{2+} and glutamate are superimposed on the density countered at 3σ. The Mg^{2+} ion is shown by a yellow sphere. The average distance between the Mg^{2+} ion and the six liganded oxygen atoms is 2.02 Å. (**B**) ATP recognition in ERS/ATP/Glu (stereo view). The ATP recognition in this complex is the same as that in ERS/ATP. (**C**) Glutamate recognition in ERS/ATP/Glu (stereo view).

ATP (Figures 4A and B, and 5A). Therefore, the non-productive arrangement of the two substrates in ERS/ATP/Glu (Figures 3A and 4A) is not due to the repulsion between the negatively charged carboxyl and phosphate groups. Thus, both the ATP and glutamate molecules can bind tightly to the GluRS substrate-binding site in the absence of $tRNA^{Glu}$, but their arrangement is non-productive. This 'dead-end' ternary complex explains simply why the amino acid activation does not occur in the absence of tRNA.

ATP binding in the presence of tRNA

The structure of ERS/tRNA/ATP has been determined at 2.4 Å resolution (Table I, Figure 1B). A comparison of this complex with that of ERS/ATP/Glu (or ERS/ATP) reveals a remarkable difference in the modes of ATP binding (Figure 4C). In ERS/tRNA/ATP, the ATP molecule binds to the catalytic pocket in a rotated orientation in the same plane, by ~37° around an axis near C2 of the adenine ring, relative to those in the ERS/ATP/Glu and ERS/ATP structures (Figures 4C and 5B).

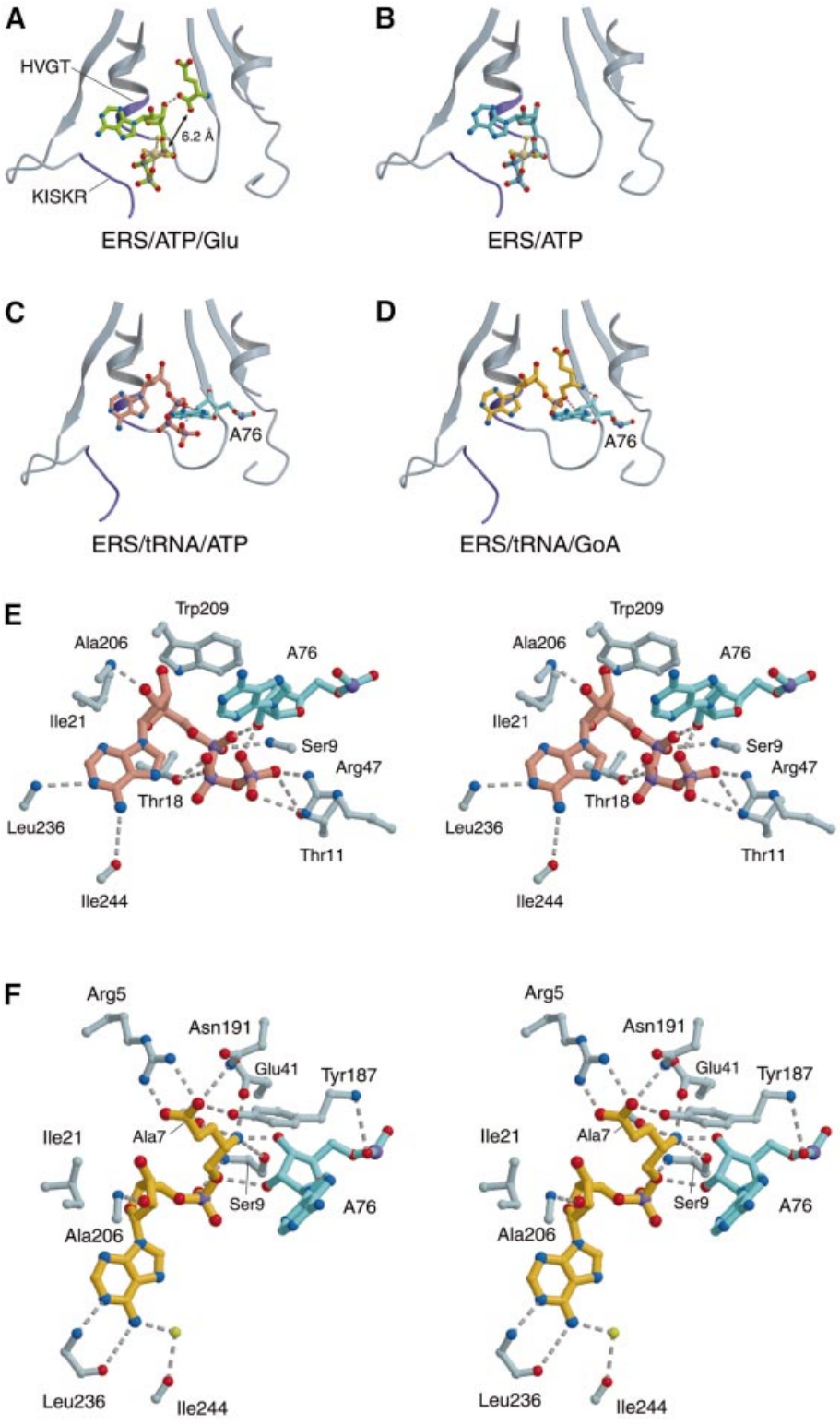

Fig. 4. Substrate/ligand(s) binding in the GluRS complexes. (A–D) The GluRS catalytic site structures in the present complexes are shown in the same orientation. The HVGT and KISKR motifs are highlighted in purple. (**A**) The ERS/ATP/Glu structure. The ATP-Mg^{2+} and glutamate molecules are shown in green. (**B**) The ERS/ATP structure. The ATP-Mg^{2+} is colored light blue. (**C**) The ERS/tRNA/ATP structure. The ATP molecule is colored salmon, and the 3′-terminal adenosine (A76) of $tRNA^{Glu}$ is cyan. (**D**) The ERS/tRNA/GoA structure. The GoA (glutamol-AMP) molecule is colored yellow. (**E**) A stereo view showing the ATP recognition in ERS/tRNA/ATP. (**F**) A stereo view showing the GoA recognition in ERS/tRNA/GoA.

In ERS/tRNA/ATP, the adenine ring is accommodated in the same hydrophobic pocket, while the base is in a different orientation (Figure 4C). The ATP ribose is largely shifted, and is docked in the depths of the active site cleft. The 2′-hydroxyl group loses the hydrogen bond with Trp209, but gains a new hydrogen bond with the amide group of Ala206 (Figure 4E). It has been reported that 2′-deoxy ATP is a poor substrate for *E.coli* GluRS

(Kern and Lapointe, 1979), which suggests that the ATP ribose binding to Ala206 is important for the reaction. The 3′-hydroxyl group of the ATP ribose interacts with a water molecule, which is bound to Arg5 and Ile204 (Supplementary figure 1C). The Ile21 side chain binds the sugar and base portions of the ATP by van der Waals contacts (Figure 4E). On the other hand, the interactions of the ATP phosphate groups with the KISKR residues (except Ile244) are missing. Instead, the ATP phosphates interact with the Thr11, Thr18 and Arg47 side chains. The $tRNA^{Glu}$ accommodates the 3′-terminal adenosine into the GluRS active site pocket by assuming a hairpin conformation in the CCA region (Figure 2B). It is remarkable that the 2′-hydroxyl group of the 3′-terminal adenosine of $tRNA^{Glu}$ (A76) hydrogen-bonds with the α- and γ-phosphates of the ATP (Figure 4E). Thus, in the presence of $tRNA^{Glu}$, the ATP molecule is located deeper in the GluRS active site cleft (Figure 4C), and is fixed in a subsite distinct from that in the absence of tRNA (Figure 4A and B). The *E.coli* GluRS exhibits practically the same dissociation constants for ATP (K_d = 90 μM) in either the absence or presence of $tRNA^{Glu}$ (Kern and Lapointe, 1979), which suggests that the ATP-binding affinities of the two subsites are almost the same.

Binding of the glutamyl-AMP analog

GoA is a stable non-hydrolyzable analog of Glu-AMP (Desjardins *et al*., 1998) (Supplementary figure 2). The stability is achieved by minimal replacement of the labile anhydride function of Glu-AMP by a phosphate ester (the C=O moiety is reduced to a CH_2). GoA belongs to the group of synthetic aminoalkyl adenylates, which are strong inhibitors of the corresponding aaRSs. It is a competitive inhibitor of the *E.coli* GluRS (K_i = 3 μM) (Desjardins *et al*., 1998). In the present study, we confirmed that GoA is also a competitive inhibitor of the *T.thermophilus* GluRS (K_i = 1.2 μM).

Based on the 2.1 Å structure of the ERS/tRNA/GoA complex (Table I), the ATP binding observed in ERS/tRNA/ATP is concluded to be 'productive' binding. The ERS/tRNA/GoA structure represents the enzyme state after the first step and before the second step of aminoacylation. In this complex, the glutamol moiety of the analog is accommodated in the same pocket as the glutamate substrate in ERS/ATP/Glu (Figures 4D and F, and 5C). The A76 ribose directly interacts with the main chain part of the glutamol moiety (Figure 4F), consistent with the previous observation that the *T.thermophilus* GluRS can discriminate glutamate from non-cognate amino acids only in the presence of $tRNA^{Glu}$ (Hara-Yokoyama *et al*., 1986). On the other hand, the adenosine moiety of GoA is in a rotated orientation, as compared with that of the ATP in the ERS/ATP/Glu and ERS/ATP structures (Figures 4D and 5C). The adenosine binding is the same as that in ERS/tRNA/ATP and, remarkably, the phosphate group of GoA is superimposed on the ATP α-phosphate (Figure 5D). In fact, the distance between the glutamate α-carboxyl oxygen in ERS/ATP/Glu and the ATP α-phosphorus in ERS/tRNA/ATP is ~2.9 Å upon superposition (Figure 5B).

Thus, GluRS possesses two modes for ATP binding, the 'non-productive' and 'productive' binding modes, which can be switched in a tRNA-dependent manner. In the absence of $tRNA^{Glu}$, the ATP-binding mode of GluRS is 'non-productive' (Figure 4A and B). GluRS, ATP and glutamate form a 'dead-end' complex (Figures 3A and 4A), which prevents Glu-AMP formation in the absence of tRNA, presumably to avoid the possible waste of the energy source on the enzyme, in the context of the instability of Glu-AMP (see above) and of the high intracellular glutamate concentration in many prokaryotes and eukaryotes (reviewed by Metzler, 1981; Csonka *et al*., 1989; Danbolt, 2001). When GluRS is in complex with $tRNA^{Glu}$, ATP can bind to the 'productive' subsite (Figure 4C) to initiate the amino acid activation, probably via a penta-covalent transition state as suggested earlier for *E.coli* GlnRS (Perona *et al*., 1993), yielding the enzyme-bound Glu-AMP (Figure 4D).

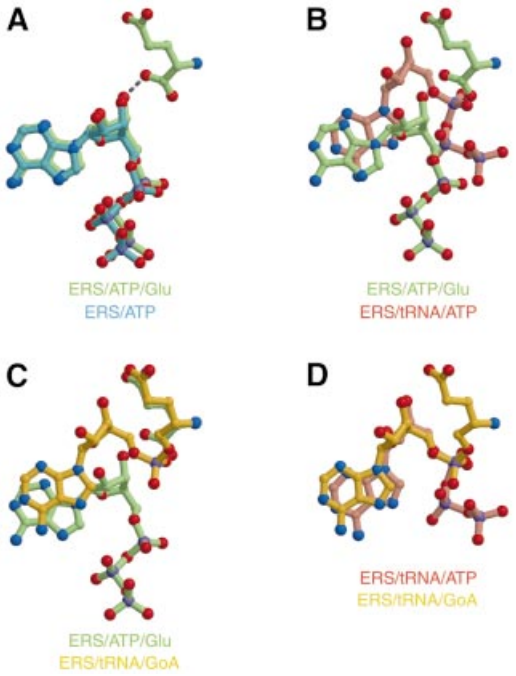

Fig. 5. Comparisons of the substrate/ligand positions among the GluRS complexes. (**A**) The ATP molecule (light blue) in ERS/ATP is compared with the ATP and glutamate (green) in ERS/ATP/Glu by superposition of the enzyme catalytic site structures. (**B**) The ATP (salmon) in ERS/tRNA/ATP is compared with the ATP and glutamate (green) in ERS/ATP/Glu by superposition. (**C**) The GoA (yellow) in ERS/tRNA/GoA is compared with the ATP and glutamate (green) in ERS/ATP/Glu by superposition. (**D**) The GoA (yellow) in ERS/tRNA/GoA is compared with the ATP (salmon) in ERS/tRNA/ATP by superposition.

Active site rearrangement within GluRS upon $tRNA^{Glu}$ binding

In order to examine how the choice is made between the two subsites for ATP binding, the ERS/ATP(/Glu) and ERS/tRNA/ATP structures were compared. The structural differences indicate that the interactions of GluRS with three regions of $tRNA^{Glu}$ are likely to account for the tRNA-dependent switching of the ATP-binding mode from 'non-productive' to 'productive'. First, the D stem of $tRNA^{Glu}$ interacts with the SC fold (Figures 2A and 6A). The SC fold domain, specific to the class Ia and Ib aaRSs, is located between the Rossmann-fold and the anticodon-binding domains, and includes the KISKR ('KMSKS') loop (Sugiura *et al*., 2000) (Figure 1). In the ERS/tRNA/

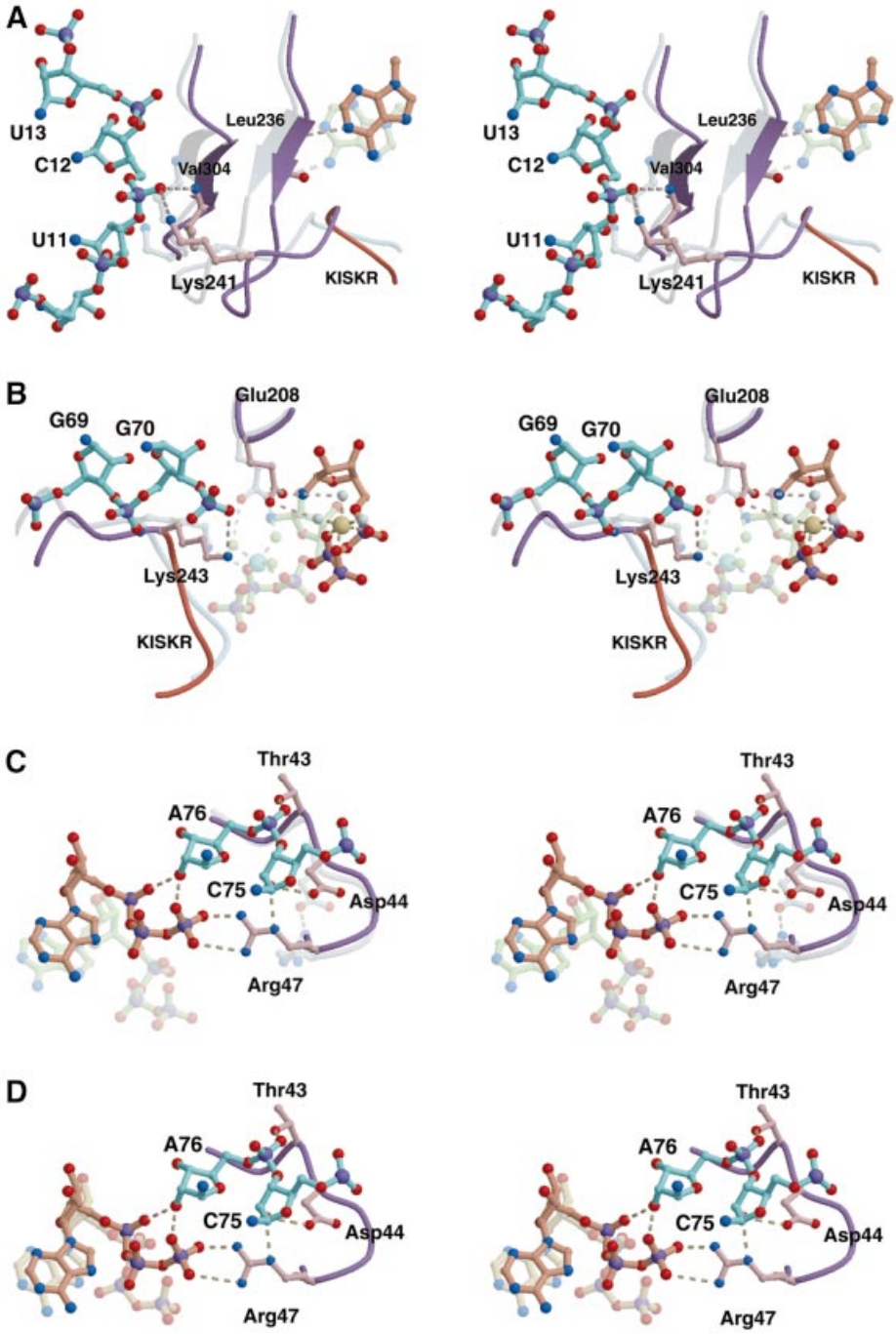

Fig. 6. Catalytic site rearrangement within GluRS upon binding with $tRNA^{Glu}$. The GluRS catalytic site structure in ERS/tRNA/ATP (purple) was compared with that in ERS/ATP (steel blue) by superposition. The ATP and portions of $tRNA^{Glu}$ in ERS/tRNA/ATP are shown in salmon and cyan, respectively, and the ATP molecule in ERS/ATP is in green. (**A**) The D stem interactions. (**B**) The acceptor stem interactions. An Mg^{2+} ion (a large yellow sphere) and its associated water molecules (light blue) are modeled for the ATP molecule in ERS/tRNA/ATP. (**C**) The 3′-CCA end interactions. (**D**) The ATP molecule (salmon) in one ERS/tRNA/ATP complex (3a) in the crystallographic asymmetric unit is compared with the ATP (beige) in the other complex (3b).

ATP structure, the backbone of nucleotide residues 10–13 in the D stem interacts with one of the β-strands (amino acid residues 301–305) and the KISKR loop of the SC fold (Figure 6A). In particular, the C12 phosphate makes hydrogen bonds with the main chain of Val304 and the side chain of Lys241. The parallel β-sheet and the KISKR loop are shifted by 1.5–2.4 Å towards the active site, as compared with their position in the tRNA-free complexes. These large shifts are likely to be due to steric hindrance between the C12 phosphate and the SC fold domain. Corresponding to the shift of the β-sheet, the adenine base changes its binding position, as Leu236 anchors the ATP adenine ring to the SC fold β-sheet in the ERS/ATP/Glu and ERS/ATP structures. The D stem of *E.coli* $tRNA^{Glu}$ contains important identity elements, U11·A24, C12·G23··C9 and U13·G22··A46, for the *E.coli* GluRS

(Sekine *et al*., 1996, 1999). It is possible that these identity elements contribute indirectly or conformationally to the specificity.

Secondly, in the ERS/tRNA/ATP structure, a region of the $tRNA^{Glu}$ acceptor stem backbone (G69–G70–U71) interacts with the KISKR loop (amino acids 241–243) (Figures 2A and 6B). The phosphate groups of G70 and U71 hydrogen-bond with the main chain and the side chain, respectively, of Lys243 (Figure 6B). These interactions result in conformational changes in the Glu208 and Lys243 side chains. In ERS/ATP/Glu and ERS/ATP, both of the residues interact with the hydrated Mg^{2+} ion, and thus, fix the ATP in the 'non-productive' position (Figure 6B). In contrast, in the ERS/tRNA/ATP structure, Lys243 is recruited to the tRNA interaction. On the other hand, Glu208 changes its side chain orientation, probably due to steric hindrance with the U71 phosphate. These tRNA-bound conformations of the Glu208 and Lys243 residues would cause steric clashes with the ATP ribose and the Mg^{2+} ion, respectively, if they were in the 'non-productive' position.

The Glu208 γ-carboxylate in the presence of tRNA is now oriented toward the triphosphate moiety of the bound ATP. This indicates that the Glu208 γ-carboxylate could retain its interaction with the putative Mg^{2+} ion in the octahedral coordination with the ATP phosphate groups and waters. This is not actually observed in the ERS/tRNA/ATP structure, probably because of the difference in the crystallization conditions, but can be modeled based on the ERS/ATP/Glu and ERS/ATP structures (Figure 6B). Therefore, this suggests that the $tRNA^{Glu}$-induced conformation change of Glu208 fixes the ATP substrate in the 'productive' position, as well as in the 'non-productive' position. Thus, the junction region of the acceptor and D helices in the L-shaped tRNA molecule plays a crucial role in the dramatic rearrangement of the GluRS structure to achieve the productive ATP binding.

Thirdly, the $tRNA^{Glu}$ 3′-CCA end binding to GluRS is important for switching the ATP binding mode. In the ERS/ATP/Glu and ERS/ATP structures, the ATP molecule does not interact with the loop region (amino acids 43–47) of GluRS, which contains the conserved residues, Thr43, Asp44 and Arg47 (Figure 6C). The Arg47 side chain is involved in a local interaction with the Asp44 side chain. In the ERS/tRNA/ATP structure, the loop of residues 43–47 accommodates the tRNA 3′-CCA end (Figures 2A and 6C). The interaction between Asp44 and Arg47 is lost upon binding with the C75 ribose, and Arg47, together with A76, directly interacts with the ATP phosphate groups. The A76 ribose seems to play a crucial role to place the ATP α-phosphate and the glutamate α-carboxyl groups in close proximity to facilitate the reaction. This is consistent with the observation that a chemical modification of the 3′ end ribose of $tRNA^{Glu}$ abolishes the GluRS activity (Ravel *et al*., 1965; Kern and Lapointe, 1979).

As mentioned above, the ERS/tRNA/ATP crystals contain two complexes (3a and 3b) of nearly the same structures in the asymmetric unit. The only remarkable differences between the two complexes are that complex 3b has a crystal contact of amino acids 50–54 of GluRS with a symmetry-related molecule, and that, in complex 3b, the 3′ end of the tRNA does not interact with the loop of residues 43–47, which assume a different conformation from that in complex 3a. Thus, the electron densities corresponding to C75 and A76 and GluRS residues 46–48 are weak in complex 3b. The location of the AMP moiety of the ATP in complex 3b is much more similar to that in the 'productive' than 'non-productive' binding mode (Figure 6D). Nevertheless, the triphosphate conformation in complex 3b is different from that in complex 3a, as the ATP γ-phosphate interactions with A76 and Arg47 are missing. This observation indicates that the tRNA-induced conformation change of the loop formed by residues 43–47, and the resultant interactions of Arg47 and A76 with the triphosphate moiety of ATP, are important to finalize the switch to the 'productive' ATP-binding mode.

Comparison with GluRSs and GlnRSs

The present complex structures have revealed both the 'productive' and 'non-productive' ATP-binding mechanisms of the *T.thermophilus* GluRS in the presence and the absence, respectively, of tRNA. To examine if these mechanisms are conserved throughout the GluRS family and in the GlnRS family, we compared their primary sequences based on GluRS and GlnRS crystal structures (Figure 7). The GluRS/GlnRS (GlxRS) superfamily can be divided into two distinct groups, based on the different structures appended to the conserved class I catalytic core (Nureki *et al*., 1995; Siatecka *et al*., 1998; Francklyn, 2001). The *T.thermophilus* GluRS is characterized by unique insertion structures in the catalytic core and α-helical anticodon-binding domains (Nureki *et al*., 1995), which are well conserved among the GluRSs from Bacteria and cellular organelles (Siatecka *et al*., 1998). In contrast, the *E.coli* GlnRS possesses different insertions in the catalytic core and β-barrel anticodon-binding domains (Rould *et al*., 1989), which are conserved among the GluRSs from Archaea and Eukarya, and all GlnRSs (from Eukarya and a few bacterial taxa). The amino acid residues characteristic of the 'productive' and 'non-productive' ATP binding in the *T.thermophilus* GluRS are almost conserved in the bacterial/organellar GluRSs (Figure 7), suggesting the conservation of the same mechanisms in this group.

Before the present structures, the *E.coli* GlnRS·$tRNA^{Gln}$·ATP complex (QRS/tRNA/ATP) (Rould *et al*., 1989) had been the only ATP-bound structure determined for the synthetases that require tRNA for amino acid activation. The manner of ATP binding in this complex is the same as that of the AMS moiety binding in the GlnRS·$tRNA^{Gln}$·QSI complex (QRS/tRNA/QSI) (Rath *et al*., 1998), suggesting that the ATP-binding mode of GlnRS in QRS/tRNA/ATP is 'productive'. Consistently, the ATP interactions characteristic of the 'productive' ATP-binding mode in ERS/tRNA/ATP are almost conserved in QRS/tRNA/ATP. In QRS/tRNA/ATP, the 2′-hydroxyl group of the ATP binds to the amide group of Thr230, corresponding to Ala206 of GluRS (Figure 7), and the ATP triphosphate moiety interacts with A76 of tRNA, and with Glu34, Asn36 and His43 of GlnRS, which correspond to Ser9, Thr11 and Thr18 of GluRS. The only exception is that Lys72 of GlnRS, corresponding to Arg47 of GluRS, does not interact with ATP in the QRS/tRNA/ATP structure, and thus the γ-phosphate conformations are

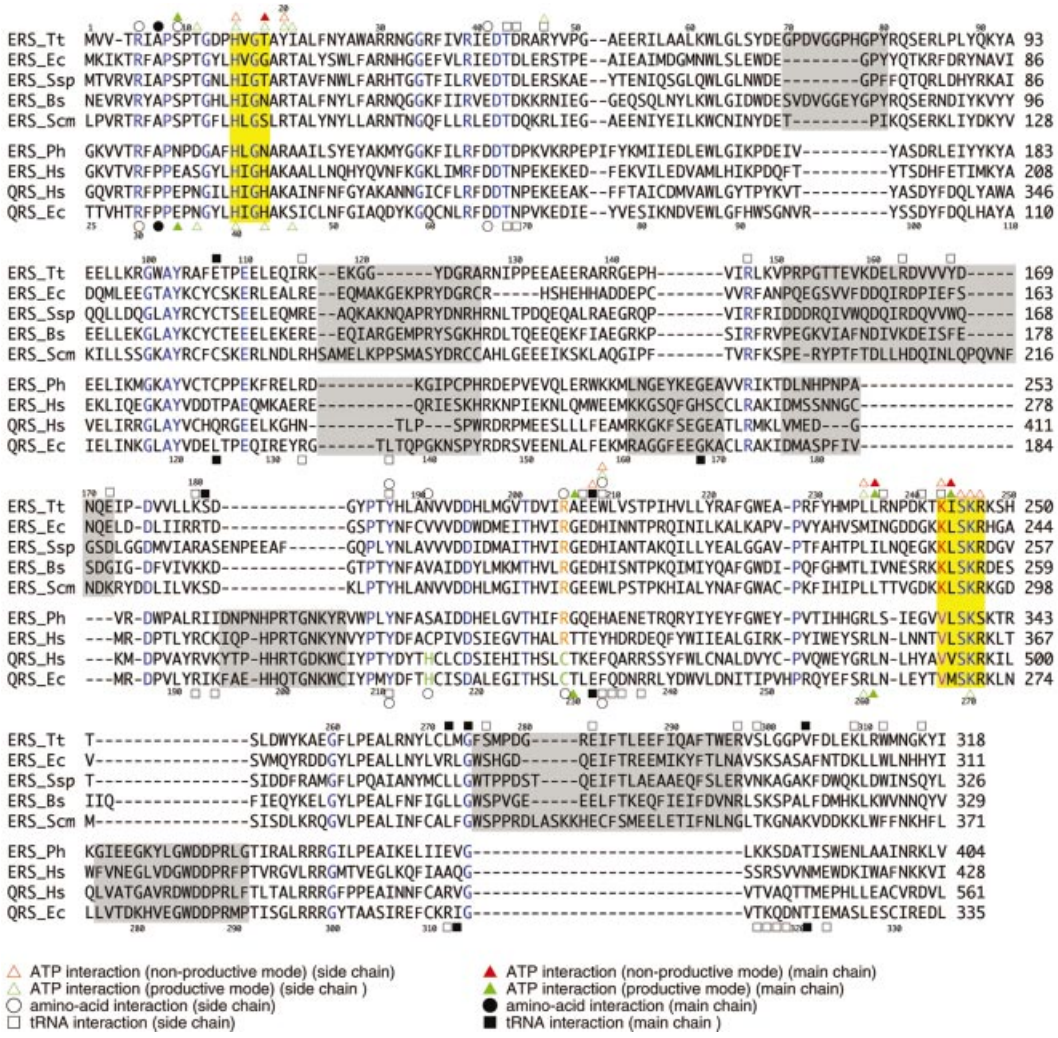

Fig. 7. Alignment of the amino acid sequences of GluRSs and GlnRSs. The amino acid sequences corresponding to the N-terminal halves (domains 1–3) of GluRSs and GlnRSs are compared based on the present *T.thermophilus* GluRS structures and *E.coli* GlnRS structures (Rould *et al*., 1989; Rath *et al*., 1998). Tt, *T.thermophilus*; Ec, *E.coli*; Ssp, *Synechocystis* sp.; Bs, *Bacillus subtilis*; Scm, *Saccharomyces cerevisiae* mitochondria; Ph, *P.horikoshii*; Hs, *Homo sapiens*. Amino acid residues conserved throughout the GlxRS family are colored blue. The 'HIGH' and 'KMSKS' motifs are highlighted in yellow. Amino acid residues conserved specifically in bacterial/organellar GluRSs are colored red, while those conserved in archaeal/eukaryal GluRSs and GlnRSs are shown in violet. The specific insertion sequences in both lineages are shown by gray zones. The GluRS- and GlnRS-specific residues for amino acid recognition are colored orange and green, respectively. Symbols above the *T.thermophilus* GluRS sequence and below the *E.coli* GlnRS sequence indicate that the marked residues are involved in the substrate interaction(s) in the structures of GluRS (the present study) and GlnRS (Rould *et al*., 1989; Rath *et al*., 1998), respectively [interactions of ATP (triangle), amino acid (circle) and tRNA (square) with the side chain (open symbol) and the main chain (closed symbol) of the protein residue]. For the ATP interactions, the 'productive' and 'non-productive' modes are indicated in green and red, respectively.

different between the QRS/tRNA/ATP and ERS/tRNA/ATP (complex 3a) structures.

The QRS/tRNA/ATP structure (Rould *et al*., 1989) also conserves the enzyme–tRNA interactions that are required for the 'productive' ATP binding in the ERS/tRNA/ATP structure. The CCA end interacts with Thr68, Asn69, Arg192, Tyr211 and Phe233, which correspond to Thr43, Asp44, Lys180, Tyr187 and Trp209, respectively, in GluRS (Figure 7). The $tRNA^{Gln}$ acceptor stem interacts with a loop region of GlnRS containing Glu232, corresponding to Glu208 in GluRS. The SC fold β-sheet of GlnRS conforms to the backbone of the tRNA D stem in QRS/tRNA/ATP, as observed in ERS/tRNA/ATP. The $tRNA^{Gln}$ C12 phosphate interacts with Thr321 of GlnRS, which corresponds to Val304 in GluRS (Figure 7). An exception is that the GlnRS 'KMSKS' motif (^{267}VMSKR^{271} in *E.coli* GlnRS) does not interact with the $tRNA^{Gln}$ acceptor stem, probably due to the lack of the first lysine residue in the motif. In GluRS, Lys243 in the KISKR motif interacts with ATP in the absence of tRNA, and with the acceptor stem in the presence of tRNA. The VMSKR motif of GlnRS is followed by a GlnRS-specific (or archaeal/eukaryal GluRS-specific) insertion structure, which interacts with a unique structural element protruding from the anticodon-binding domain (Rould *et al*., 1989, 1991). We speculate that GlnRS may have acquired these elements to compensate for the lack of the first lysine residue in the 'KMSKS' motif.

On the other hand, the ATP-binding manner of GlnRS in the absence of $tRNA^{Gln}$ remains unclear, as the tRNA-free GlnRS structure is not available. In the ERS/ATP/Glu and ERS/ATP structures, the 'non-productive' ATP-binding subsite is characterized by extensive interactions of the ATP phosphate groups with Lys243, Ile244, Ser245, Lys246 and Arg247 in the KISKR motif (Figure 3B). These residues, except for the first lysine residue, are fundamentally conserved in the GlnRS VMSKR motif (Figure 7). However, except for Lys270, the roles of these conserved residues in GlnRS are not understood. Based on the conserved enzyme–tRNA and enzyme (or tRNA)–ATP interactions in the 'productive' mode, and on the conserved protein residues characteristic of the 'non-productive' ATP-binding mode, there is a possibility that GlnRS can switch its ATP-binding modes in a tRNA-dependent manner, as observed for GluRS. It is remarkable that the other members of the archaeal/eukaryal GluRSs and all of the GlnRSs conserve most of the amino acid residues described here for the GlnRS structure (Figure 7).

Relevance to the reaction mechanism

A steady-state kinetic study of the *E.coli* GluRS indicated that ATP and $tRNA^{Glu}$ bind randomly to the free enzyme, and then glutamate binds to the ternary ERS/tRNA/ATP complex (Kern and Lapointe, 1981). This indicates that GluRS first forms either the ERS/tRNA or the ERS/ATP complex, and then the ERS/tRNA/ATP complex is formed. In the presence of a saturating $tRNA^{Glu}$ concentration (GluRS completely bound with tRNA), the kinetic property of GluRS is that of a rapidly equilibrated bireactant (ATP and glutamate) system. On the other hand, when ATP is saturating and the $tRNA^{Glu}$ concentration is low (most GluRS bound with ATP), the system is not in a rapid equilibrium, and it has been suggested that the tRNA-induced conformational change is rate determining (Kern and Lapointe, 1981). If the catalytic properties of the *T.thermophilus* GluRS are similar to those of the *E.coli* GluRS, then they are consistent with the *T.thermophilus* GluRS complex structures reported here and previously (Sekine *et al*., 2001). The active site structure of GluRS does not change upon ATP binding by ERS/tRNA, but would be shifted from the non-productive state to the productive state upon tRNA binding by ERS/ATP. On the other hand, it is not clear whether or not the ERS/ATP/Glu can directly shift to the quaternary complex upon tRNA binding, which will require further studies.

How does glutamate bind to the active site formed on ERS/tRNA/ATP? In complex 3a (one of the two ERS/tRNA/ATP complexes in the asymmetric unit) (Figure 6D), the tRNA A76 cooperates with the bound ATP to form the lid of the glutamate-binding site (the closed conformation of the 3′ terminus), which appears to prevent glutamate from entering into this site. On the other hand, in the other complex (complex 3b), C75 and A76 are not well ordered, and the ATP is in a slightly different position, as described above (the semi-closed conformation) (Figure 6D). Furthermore, in the ERS/tRNA complex (Sekine *et al*., 2001), C75 and A76 are completely disordered (the open conformation). These observations suggest that the tRNA 3′ terminus is flexible enough to assume the open conformation that allows glutamate to enter into its binding site. Possibly, the 3′ terminus then shifts to the closed conformation, while Glu-AMP is formed. Actually, in the ERS/tRNA/GoA structure, A76 interacts with both the AMP and the glutamol moieties in the closed conformation (Figure 4F).

Based on the present structures, we made a plausible model of the putative quaternary complex of GluRS, $tRNA^{Glu}$, ATP and glutamate (not shown). The glutamate molecule observed in the ERS/ATP/Glu structure was placed in the ERS/tRNA/ATP (complex 3a) structure. As one of the α-carboxyl oxygens of the modeled glutamate causes a steric clash with one of the ATP α-phosphate oxygens (Figure 5B), the modeled glutamate molecule was rotated slightly to avoid the steric hindrance of the α-carboxylate group, while retaining the essential recognitions of the γ-carboxyl and α-ammonium groups. In this model, the glutamate α-carboxyl group is free from any interaction with GluRS and tRNA, which is favorable for the reaction. The free nucleophilic oxygen of the glutamate α-carboxylate, the ATP α-phosphorus and the leaving oxygen of the ATP α-phosphate are nearly coaxial, which is reasonable to achieve the initial amino acid activation via an in-line displacement. On the other hand, as the 2′-hydroxyl group of A76 is close to the methylene group of the GoA phosphate ester linkage in the ERS/tRNA/GoA structure, the activated glutamyl group might be transferred immediately to the 2′-hydroxyl group after Glu-AMP formation.

It should be noted that, in the ERS/tRNA/ATP and ERS/tRNA/GoA structures, the latter half of the enzyme KISKR loop (residues 245–250) is in an 'open' conformation (probably due to extensive water-mediated crystal contacts), and does not interact with ATP or tRNA. In contrast, in the QRS/tRNA/ATP structure (Rould *et al*., 1989), the corresponding loop region is in a 'closed' conformation, and Lys270 (the second 'KMSKS' lysine) interacts with the ATP α-phosphate. This lysine residue has been proposed to stabilize the transition state of the first reaction step (Perona *et al*., 1993). We could readily model a 'closed' conformation of the GluRS KISKR loop by its simple translation as a rigid body (not shown), and therefore we propose a similar role for Lys246.

Materials and methods

Determination of the K_i of glutamol-AMP against T.thermophilus GluRS

The aminoacylation reactions were performed at 65°C in 50 mM HEPES–NaOH buffer pH 7.5, containing 16 mM $MgCl_2$, 4 mM ATP, 12 mM tRNA and various concentrations of L-glutamate (50–600 mM). Instead of the *T.thermophilus* $tRNA^{Glu}$, a purified *E.coli* $tRNA^{Glu}$ sample (Madore *et al*., 1999) was used for the K_i determination, as *E.coli* $tRNA^{Glu}$ is comparable with *T.thermophilus* $tRNA^{Glu}$ as a substrate of the *T.thermophilus* GluRS (the K_m values are 0.60 and 0.65 μM for *E.coli* and *T.thermophilus* $tRNA^{Glu}$, respectively) (Hara-Yokoyama *et al*., 1984). For the K_i determination, the K_m and k_{cat} values were estimated in the absence and presence of 0.5, 1 and 2 mM of glutamol-AMP. Data were analyzed with Lineweaver–Burk and Dixon plots.

Cloning of T.thermophilus $tRNA^{Glu}$

The structural gene for $tRNA^{Glu}$ was isolated from the *T.thermophilus* genome, and its primary sequence was determined: 5′-GGCCCCATCGTCTAGCGGTTAGGACGCGGCCCTCTCAAGGCCGAAACGGGGGTTCGATTCCCCCTGGGGTCACCA-3′. This $tRNA^{Glu}$ is an isoacceptor with the CUC anticodon, and has 79% sequence identity with the *E.coli* $tRNA^{Glu}$. The $tRNA^{Glu}$ identity elements for GluRS in the *E.coli* system are G1·C72, U2·A71, C4·G49, U34, U35, C36, A37, U11·A24,

C12·G23··C9, U13·G22··A46, and the lack of residue 47 (Sekine *et al*., 1996, 1999). The *T.thermophilus* $tRNA^{Glu}$ conserves these elements, except that it has G2·U71 and C34 instead of U2·A71 and U34, respectively. As described above, the *T.thermophilus* GluRS can aminoacylate both the *E.coli* and *T.thermophilus* $tRNA^{Glu}$ species with similar efficiencies. The glutamate-accepting activity of the *E.coli* $tRNA^{Glu}$ transcript with the *T.thermophilus* GluRS was decreased by mutations of the conserved identity elements, but not by the mutation of U34 to C (S.Sekine and S.Yokoyama, unpublished).

Purification and crystallization

The *T.thermophilus* $tRNA^{Glu}$ gene was cloned with the T7 promoter into the vector pUC118, and was used as a template for transcription with T7 RNA polymerase. The procedures for *in vitro* transcription and for purification of the transcript were described (Sekine *et al*., 1996, 2001). This $tRNA^{Glu}$ transcript is a good substrate for the *T.thermophilus* GluRS. The K_m value of the transcript was determined to be 1.4 μM (S.Sekine and S.Yokoyama, unpublished). *Thermus thermophilus* GluRS was over-expressed in *E.coli* BL21(DE3), and was purified as described previously (Nureki *et al*., 1995).

The ERS/ATP/Glu co-crystals were obtained by equilibrating an 8 μl drop, containing 5.0 mg/ml GluRS in 10 mM MOPS-Na buffer pH 6.5 with 5 mM $MgCl_2$, 2.5 mM 2-mercaptoethanol, 1% polyethylene glycol (PEG) 6000, 2 mM ATP and 2 mM glutamate, against a 1 ml reservoir solution containing 10% PEG at either 4 or 20°C. They belong to the space group $P2_12_12_1$ with unit cell dimensions a = 81.92, b = 82.62 and c = 83.11 Å (Table I). This crystal form is different from that of the free GluRS crystals, which belong to the space group $P2_12_12_1$, with unit cell dimensions a = 75.8, b = 110.1 and c = 67.6 Å (Nureki *et al*., 1995). There is one GluRS molecule in the asymmetric unit. The ERS/ATP co-crystals (Table I) were grown under the same conditions, but without glutamate in the drop. The ERS/tRNA/ATP and ERS/tRNA/GoA crystals (Table I) were obtained by adding 1 mM ATP and 0.5 mM GoA, respectively, to the hanging drops containing the ERS/tRNA binary complex crystals (Sekine *et al*., 2001). After an incubation at 20°C for 3 days or more, these crystals were subjected to diffraction data collection.

Data collection and structure determination

All of the diffraction data were collected with frozen crystals at 100 K, using synchrotron radiation at the SPring-8 beamlines (Hyogo, Japan) (Table I). The data were processed with the programs DENZO and SCALEPACK (Otwinowski and Minor, 1997). The ERS/ATP/Glu and ERS/ATP complex structures were solved using the tRNA-free GluRS structure (Nureki *et al*., 1995) as the starting model. The coordinates of the ERS/tRNA binary complex structure (Sekine *et al*., 2001) were used for the determination of the ERS/tRNA/ATP and ERS/tRNA/GoA complex structures. Each model was fitted manually to the electron density using the program O (Jones *et al*., 1991). The refinements were carried out with the CNS program (Brünger *et al*., 1998) (Table I). Stereochemical qualities of the refined models were estimated by Ramachandran plots calculated by the program PROCHECK (Laskowski, 1993).

Structure data

The atomic coordinates and structure factors have been deposited at the RCSB Protein Data Bank (PDB ID 1J09 for ERS/ATP/Glu, 1N75 for ERS/ATP, 1N77 for ERS/tRNA/ATP, and 1N78 for ERS/tRNA/GoA).

Supplementary data

Supplementary data are available at *The EMBO Journal* Online.

Acknowledgements

We thank Y.Kawano, T.Kumasaka, M.Yamamoto, M.Kawamoto and N.Kamiya for supporting our data collections at the SPring-8 beamlines, and D.Kern for helpful discussions about GluRS kinetics. This work was supported in part by a grant from the RIKEN Special Postdoctoral Researchers Program to S.S., by the Fonds pour la Formation de Chercheurs et l'Aide à la Recherche du Québec (FCAR) to R.C. and J.L. (D.Y.D. was a FCAR doctoral fellow), and by Grants-in-Aid for Science Research on Priority Areas from the Ministry of Education, Science, Sports and Culture of Japan to S.Y.

References

Brünger,A.T. *et al*. (1998) Crystallography and NMR system: a new software suite for macromolecular structure determination. *Acta Crystallogr. D*, **54**, 905–921.

Cavarelli,J., Delagoutte,B., Eriani,G., Gangloff,J. and Moras,D. (1998) L-Arginine recognition by yeast arginyl-tRNA synthetase. *EMBO J.*, **17**, 5438–5448.

CCP4 (1994) The CCP4 suite: programs for protein crystallography. *Acta Crystallogr. D*, **50**, 760–763.

Csonka,L.N. (1989) Physiological and genetic responses of bacteria to osmotic stress. *Microbiol. Rev.*, **53**, 121–147.

Cusack,S. (1995) Eleven down and nine to go. *Nat. Struct. Biol.*, **2**, 824–831.

Danbolt,N.C. (2001) Glutamate uptake. *Prog. Neurobiol.*, **65**, 1–105.

Delagoutte,B., Moras,D. and Cavarelli,J. (2000) tRNA aminoacylation by arginyl-tRNA synthetase: induced conformations during substrates binding. *EMBO J.*, **19**, 5599–5610.

Desjardins,M., Garneau,S., Desgagnés,J., Lacoste,L., Yang,F., Lapointe,J. and Chênevert,R. (1998) Glutamyl adenylate analogues are inhibitors of glutamyl-tRNA synthetase. *Bioorg. Chem.*, **26**, 1–13.

Deutscher,M.P. (1967) Rat liver glutamyl ribonucleic acid synthetase. II. Further properties and anomalous pyrophosphate exchange. *J. Biol. Chem.*, **242**, 1132–1139.

Eriani,G., Delarue,M., Poch,O., Gangloff,J. and Moras,D. (1990) Partition of tRNA synthetases into two classes based on mutually exclusive sets of sequence motifs. *Nature*, **347**, 203–206.

Francklyn,C.S. (2001) Charging two for the price of one. *Nat. Struct. Biol.*, **8**, 189–191.

Hara-Yokoyama,M., Yokoyama,S. and Miyazawa,T. (1984) Purification and characterization of glutamyl-tRNA synthetase from an extreme thermophile, *Thermus thermophilus* HB8. *J. Biochem.*, **96**, 1599–1607.

Hara-Yokoyama,M., Yokoyama,S. and Miyazawa,T. (1986) Conformation change of $tRNA^{Glu}$ in the complex with glutamyl-tRNA synthetase is required for the specific binding of L-glutamate. *Biochemistry*, **25**, 7031–7036.

Ibba,M., Bono,J.L., Rosa,P.A. and Söll,D. (1997a) Archaeal-type lysyl-tRNA synthetase in the Lyme disease spirochete *Borrelia burgdorferi*. *Proc. Natl Acad. Sci. USA*, **94**, 14383–14388.

Ibba,M., Morgan,S., Curnow,A.W., Pridmore,D.R., Vothknecht,U.C., Gardner,W., Lin,W., Woese,C.R. and Söll,D. (1997b) A euryarchaeal lysyl-tRNA synthetase: resemblance to class I synthetases. *Science*, **278**, 1119–1122.

Ibba,M., Losey,H.C., Kawarabayasi,Y., Kikuchi,H., Bunjun,S. and Söll,D. (1999) Substrate recognition by class I lysyl-tRNA synthetases: a molecular basis for gene displacement. *Proc. Natl Acad. Sci. USA*, **96**, 418–423.

Jones,T.A., Zou,J.-Y., Cowan,S.W. and Kjeldgaard,M. (1991) Improved methods for building protein models in electron density maps and the location of errors in these models. *Acta Crystallogr. A*, **47**, 110–119.

Kern,D. and Lapointe,J. (1979) Glutamyl transfer ribonucleic acid synthetase of *Escherichia coli*. Study of the interactions with its substrates. *Biochemistry*, **18**, 5809–5818.

Kern,D. and Lapointe,J. (1980) The catalytic mechanism of glutamyl-tRNA synthetase of *E.coli*. *Eur. J. Biochem.*, **106**, 137–150.

Kern,D. and Lapointe,J. (1981) The catalytic mechanism of glutamyl-tRNA synthetase of *Escherichia coli*. A steady-state kinetic investigation. *Eur. J. Biochem.*, **115**, 29–38.

Kraulis,P.J. (1991) MOLSCRIPT: a program to produce both detailed and schematic plots of protein structures. *J. Appl. Crystallogr.*, **24**, 946–950.

Lapointe,J. and Söll,D. (1972) Glutamyl transfer ribonucleic acid synthetase of *Escherichia coli*. I. Purification and properties. *J. Biol. Chem.*, **247**, 4966–4974.

Laskowski,R.A., MacArthur,M.W., Moss,D.S. and Thornton,J.M. (1993) PROCHECK: a program to check the stereochemical quality of protein structures. *J. Appl. Crystallogr.*, **26**, 283–291.

Lee,L.W., Ravel,J.M. and Shive,W. (1967) A general involvement of acceptor ribonucleic acid in the initial activation step of glutamic acid and glutamine. *Arch. Biochem. Biophys.*, **121**, 614–618.

Madore,E., Florentz,C., Giegé,R., Sekine,S., Yokoyama,S. and Lapointe,J. (1999) Effect of modified nucleotides on *Escherichia coli* $tRNA^{Glu}$ structure and on its aminoacylation by glutamyl-tRNA synthetase. Predominant and distinct roles of the mnm^5 and s^2 modifications of U34. *Eur. J. Biochem.*, **266**, 1128–1135.

Mehler,A.H. and Mitra,K. (1967) The activation of arginyl transfer

ribonucleic acid synthetase by transfer ribonucleic acid. *J. Biol. Chem.*, **242**, 5495–5499.
Merritt,E.A. and Murphy,M.E.P. (1994) Raster3D version 2.0: a program for photorealistic molecular graphics. *Acta Crystallogr. D*, **50**, 869–873.
Metzler,H. (1981) Light-induced oscillations of the glutamate pool size and of the respiratory oxygen uptake in the blue–green alga *Anacystis nidulans*. *Z. Allg. Mikrobiol.*, **21**, 323–327.
Mitra,K. and Mehler,A.H. (1966) The role of transfer ribonucleic acid in the pyrophosphate exchange reaction of arginine-transfer ribonucleic acid synthetase. *J. Biol. Chem.*, **241**, 5161–5162.
Mitra,S.K. and Mehler,A.H. (1967) The arginyl transfer ribonucleic acid synthetase of *Escherichia coli*. *J. Biol. Chem.*, **242**, 5490–5494.
Nureki,O., Vassylyev,D.G., Katayanagi,K., Shimizu,T., Sekine,S., Kigawa,T., Miyazawa,T., Yokoyama,S. and Morikawa,K. (1995) Architectures of class-defining and specific domains of glutamyl-tRNA synthetase. *Science*, **267**, 1958–1965.
Otwinowski,Z. and Minor,W. (1997) Processing of X-ray diffraction data collected in oscillation mode. *Methods Enzymol.*, **276**, 307–326.
Perona,J.J., Rould,M.A. and Steitz,T.A. (1993) Structural basis for transfer RNA aminoacylation by *Escherichia coli* glutaminyl-tRNA synthetase. *Biochemistry*, **32**, 8758–8771.
Rath,V.L., Silvian,L.F., Beijer,B., Sproat,B.S. and Steitz,T.A. (1998) How glutaminyl-tRNA synthetase selects glutamine. *Structure*, **6**, 439–449.
Ravel,J.M., Wang,S.-F., Heinemeyer,C. and Shive,W. (1965) Glutamyl and glutaminyl ribonucleic acid synthetases of *Escherichia coli* W. Separation, properties and stimulation of adenosine triphosphate–pyrophosphate exchange by acceptor ribonucleic acid. *J. Biol. Chem.*, **240**, 432–438.
Rould,M.A., Perona,J.J., Söll,D. and Steitz,T.A. (1989) Structure of *E.coli* glutaminyl-tRNA synthetase complexed with $tRNA^{Gln}$ and ATP at 2.8 Å resolution. *Science*, **246**, 1135–1142.
Rould M.A., Perona J.J. and Steitz,T.A. (1991) Structural basis of anticodon loop recognition by glutaminyl-tRNA synthetase. *Nature*, **352**, 213–218.
Sekine,S. *et al*. (1996) Major identity determinants in the 'augmented D helix' of $tRNA^{Glu}$ from *Escherichia coli*. *J. Mol. Biol.*, **256**, 685–700.
Sekine,S., Nureki,O., Tateno,M. and Yokoyama,S. (1999) The identity determinants required for the discrimination between $tRNA^{Glu}$ and $tRNA^{Asp}$ by glutamyl-tRNA synthetase from *Escherichia coli*. *Eur. J. Biochem.*, **261**, 354–360.
Sekine,S., Nureki,O., Shimada,A., Vassylyev,D.G. and Yokoyama,S. (2001) Structural basis for anticodon recognition by discriminating glutamyl-tRNA synthetase. *Nat. Struct. Biol.*, **8**, 203–206.
Shimada,A., Nureki,O., Goto,M., Takahashi,S. and Yokoyama,S. (2001) Structural and mutational studies of the recognition of the arginine tRNA-specific major identity element, A20, by arginyl-tRNA synthetase. *Proc. Natl Acad. Sci. USA*, **98**, 13537–13542.
Siatecka,M., Rozek,M., Barciszewski,J. and Mirande,M. (1998) Modular evolution of the Glx-tRNA synthetase family. Rooting of the evolutionary tree between the bacteria and archaea/eukarya branches. *Eur. J. Biochem.*, **256**, 80–87.
Sugiura,I. *et al*. (2000) The 2.0 Å crystal structure of *Thermus thermophilus* methionyl-tRNA synthetase reveals two RNA-binding modules. *Struct. Fold. Design*, **8**, 197–208.
Terada,T., Nureki,O., Ishitani,R., Ambrogelly,A., Ibba,M., Söll,D. and Yokoyama,S. (2002) Functional convergence of two lysyl-tRNA synthetases with unrelated topologies. *Nat. Struct. Biol.*, **9**, 257–262.

Received July 12, 2002; revised November 25, 2002; accepted December 3, 2002